

Formation of Long, Multicenter π -[TCNE] $_2^{2-}$ Dimers in Solution: Solvation and Stability Assessed through Molecular Dynamics Simulations

Marçal Capdevila-Cortada,^{a,b,c} Jordi Ribas-Arino,^{a,*} Alain Chaumont,^b Georges Wipff,^b and Juan J. Novoa^a

(a) Departament de Química Física and IQTCUB, Facultat de Química, Universitat de Barcelona, Av. Diagonal 645, 08028 Barcelona (Spain); (b) Laboratoire MSM, UMR CNRS 7140, Institut de Chimie, 4 rue B. Pascal, 67 000 Strasbourg (France); (c) Current address: Institute of Chemical Research of Catalonia (ICIQ), The Barcelona Institute of Science and Technology, Av. Països Catalans 16, 43007 Tarragona (Spain).

Abstract: Purely organic radical-ions dimerize in solution at low temperature forming long, multicenter bonds, despite the metastability of the isolated dimers. Here, we present the first computational study of these π -dimers in solution, with explicit consideration of solvent molecules and finite temperature effects. By means of force-field and *ab initio* molecular dynamics and free energy simulations, the structure and stability of π -[TCNE] $_2^{2-}$ dimers in dichloromethane have been evaluated. While dimers dissociate at room temperature, they are stable at 175 K and their structure is similar to the one in the solid-state, with a cofacial arrangement of the radicals at an interplanar separation of ca. 3.0 Å. The π -[TCNE] $_2^{2-}$ dimers form dissociated ion pairs with the NBu_4^+ counterions, and their first solvation shell comprises ca. 20 CH_2Cl_2 molecules. Among them, the 8 molecules distributed along the equatorial plane of the dimer play a key role in stabilizing the dimer via bridging C-H \cdots N contacts. The calculated free energy of dimerization of TCNE $^{\cdot-}$ in solution at 175 K is $-5.5 \text{ kcal mol}^{-1}$. These results provide the first quantitative model describing the pairing of radical-ions in solution, and demonstrate the key role of solvation forces on the dimerization process.

Introduction

Organic acceptor (or donor) compounds such as tetracyanoethylene, TCNE, once reduced (or oxidized) may form diamagnetic dimers that exhibit long, multicenter bonding.^[1,2] This bond arises from the overlap of the SOMO orbitals of [TCNE] $^{\cdot-}$ to form a doubly-occupied bonding and an empty antibonding combinations, leading to the diamagnetic π -[TCNE] $_2^{2-}$ species.^[1] The long, multicenter bonded π -[TCNE] $_2^{2-}$ dimer, which exhibits an intermonomer bonding distance of $\sim 2.9 \text{ \AA}$ (see Figure 1), was early experimentally observed^[3,4] and theoretically characterized a few decades later.^[5-7] Further studies in dichloromethane solution at low temperature determined its equilibrium constant K_D and enthalpy and entropy of dimerization (ΔH_D and ΔS_D) by UV-vis and EPR measurements.^[8] Other organic radicals have been shown to exhibit long, multicenter bonding; e.g. other radical anions such as reduced tetracyanobenzene (TCNB $^{\cdot-}$)^[9] or 7,7,8,8-tetracyano-*p*-quinodimethane (TCNQ $^{\cdot-}$),^[10-12] radical cations such as oxidized tetrathiafulvalene (TTF $^{\cdot+}$),^[13,14] or neutral radicals such as phenalenyl derivatives.^[15,16] Long, multicenter bonding has also been observed in the zwitterionic π -[TTF $^{\delta+}\cdots\text{TCNE}^{\delta-}$] charge-transfer dyad.^[17]

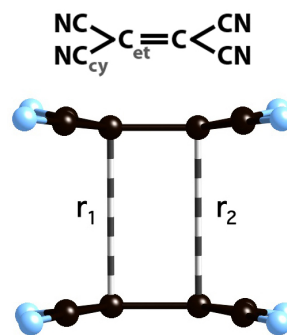


Figure 1. (top) TCNE scheme with the labeling used along this work. (bottom) π -[TCNE] $_2^{2-}$ dimer structure extracted from the $[\text{NBu}_4][\text{TCNE}]$ crystal. The r_1 and r_2 distances are also used to define the reaction coordinate r'_{\cdot} .

Salts of the aforementioned organic radical ions are well known to exhibit technologically significant properties like magnetic ordering,^[18] metal-like electrical conductivity,^[19] and superconductivity.^[20] For instance, TCNE,^[21] TCNQ,^[22] and TCNP,^[23] are employed as building blocks in molecule-based bulk ferromagnets with magnetic ordering temperatures above room temperature. In the context of molecule-based materials, the formation of long, multicenter dimers is usually considered undesirable because the resulting electron pairing is detrimental to these physical properties. However, the π -dimerization is not always disadvantageous because a weak

dimerization in the solid state can give rise to materials that can switch between two phases, one containing dimers and the other the monomeric radicals.^[24] Given the different magnetic, conducting and optical properties of the dimeric and monomeric phases, these materials are promising candidates for possible magneto-optical and magneto-electronic devices. On the other hand, long, multicenter dimerization was also recently detected in supramolecular aggregates at room temperature.^[25–30] These aggregates constitute an emerging class of potential systems for molecular switching applications.^[31] In view of the increasingly acknowledged potential applications of long, multicenter dimers of ionic radicals, it is of high importance to achieve a complete understanding of the factors that control their formation and the nature of their interactions.

Previous quantum mechanical (QM) studies^[32–34] showed that in the gas phase long, multicenter bonds between isolated radical ions are metastable, since the dispersion and bonding stabilizing terms cannot overcome the coulombic repulsive term. However, they do form in the solid state and in solution. In the solid state, the stability of long, multicenter dimerization can be rationalized by means of (cation)₂(anion)₂ aggregates, where the sum of cation⋯anion attractions is larger in magnitude than the sum of cation⋯cation and anion⋯anion repulsions.^[35] The structure of these aggregates is such that they allow the formation of long, multicenter bonds between their radical-ions.^[8] In some of these aggregates, e.g. K₂TCNE₂, the presence of the preferred angular orientations between the radical ions and their dependence on the cations was evaluated.^[33,35,36]

In solution, the long, multicenter dimerization of radical ions was experimentally detected at low temperatures, as in the case of π -[TCNE]₂²⁻ dimers in dichloromethane (hereafter referred as DCM) below -83° C.^[8] At room temperature, the π -dimers dissociate into their constituting radical ions.^[8] It was also shown that the thermodynamic magnitudes characterizing the dimerization remain unaffected by the size or nature of the counterion.^[8,37] Based on QM calculations, the presence of long, multicenter bonds in solution was first qualitatively explained for π -[TCNE]₂²⁻ dimers in DCM in terms of stable π -[TCNE]₂²⁻(CH₂Cl)₄ aggregates.^[38] Using analogous [radical ion]₂(solvent)_n microsolvated cluster models, the presence of long-bonded π -[TCNQ]₂²⁻ and π -[TTF]₂²⁺ dimers in DCM solutions was also rationalized.^[39,40] According to these calculations, the aggregates are energetically stable against dissociation into the isolated radicals and solvent molecules,^[35,38,39] in agreement with experimental evidence in solution. Their stability arises from the energetically favorable [radical ion]⋯solvent interactions present in the aggregate, which overcome the repulsive [radical ion]⋯[radical ion] interaction.^[38] Furthermore, it was observed that in their stable local minima, the radical ions preserve the same cofacial arrangement as in crystals. Similar conclusions (in terms of stability and geometry) were reached using continuum models of solvation.^[41,42]

Notwithstanding the valuable insight provided by the microsolvated cluster models, their use in

modeling the solution can be questioned. Indeed, the number of solvent molecules included in these models is just the minimum number of molecules that render the aggregate stable. Besides, the geometry optimizations of the aggregates were carried out using one single initial configuration, in which the radicals of the π -dimer were placed in a cofacial arrangement (as inferred from the fact that UV-vis spectra of radical-ion solutions are similar to the spectra of their corresponding π -dimerized crystals), and the solvent molecules were placed at the energetically most stable positions, without systematic exploration of the potential energy surface of these aggregates. Furthermore, entropy effects, which are known to be crucial for ion pairing in solution (e.g., for the dimerization of TCNE^{•-} in dichloromethane at 175 K, the favorable enthalpy term, $\Delta H = -8.8$ kcal mol⁻¹, is counterbalanced by a high antagonistic entropy term $T\Delta S = -7.2$ kcal mol⁻¹)^[8] were not considered in the QM calculations of microsolvated cluster models.

Given the shortcomings of these microsolvated model systems, there are several key issues regarding ionic radicals in solution that remain unsettled: i) does their cofacial arrangement correspond to the lowest-lying configuration of the dimer? ii) are the π -dimers stable against their dissociation into two solvated monomers? iii) what is the solvent structure around the π -dimer? iv) do the counterions form contact ion pairs with the radicals and/or with the π -dimer? v) do the counterions contribute to the stability of the π -dimer? and vi) which is the role of solvation forces in facilitating the approach of the like-charged ionic radicals before the stabilizing orbital interactions start acting? It is clear that a full understanding of the intriguing phenomenon of organic radical ions pairing in solution cannot be achieved until these questions are addressed. Achieving this understanding is not only important from a fundamental point of view (in connection with the pairing of like-charged closed-shell organic ions),^[43–49] but it is also very important in the context of molecule-based materials, where π -dimers in solution may act as building blocks precursors of the grown crystals.

In this work, we will provide an answer to the aforementioned questions by means of the first computational investigation in which the solvation of ionic radicals is studied in solution with an explicit consideration of the solvent molecules and finite temperature (dynamics) effects. For such a task, two complementary molecular dynamic approaches were used: force-field molecular dynamics (FFMD) and *ab initio* molecular dynamics (AIMD), which are based on a force field and a QM *ab initio* representation of the potential energy, respectively. The former does not account for the bonding component between radical ions that originates from the SOMO/SOMO overlap, while the latter takes this into account. The particular system studied here is the π -dimerization of TCNE^{•-} in DCM solution. FFMD simulations are used here to assess whether the NBu₄⁺ counterions (used in the exhaustive experimental study of Ref. [8]) form contact ion pairs with the TCNE^{•-} radical or with the [TCNE]₂²⁻ dimer, and whether they contribute to the stability of the dimer. FFMD simulations will also allow us to determine the

effective “non-covalent” interaction between two TCNE^{•-} anions in solution, in the absence of intermolecular orbital overlap. AIMD simulations, in turn, are used here to depict the structure and solvation of the dimer, and the free energy profile for its dissociation in solution. The simulated temperatures are 175 K, where the dimer is experimentally observed, and 300 K, where the dimer is fully dissociated.^[8]

Methodological Details

In the classical force field MD (FFMD) simulations carried out in this work, intermolecular interactions are assumed to be of electrostatic (coulombic) and van der Waals type, (i.e., without accounting for changes in polarization, charge transfer, and orbital interactions along the dynamics). These simulations were performed using the AMBER 10 software,^[50] where the potential energy U is described by a sum of bond, angle, and dihedral deformation energies and pairwise additive 1-6-12 interactions between non-bonded atoms (electrostatic and van der Waals terms).

$$U = \sum_{bonds} K_r (r - r_{eq})^2 + \sum_{angles} K_\theta (\theta - \theta_{eq})^2 + \sum_{dihedrals} \sum_n V_n (1 + \cos(n\phi)) + \sum_{i < j} \left(\frac{q_i q_j}{R_{ij}} - 2\epsilon_{ij} \left(\frac{R_{ij}^*}{R_{ij}} \right)^6 + \epsilon_{ij} \left(\frac{R_{ij}^*}{R_{ij}} \right)^{12} \right)$$

Cross terms in van der Waals interactions were constructed using the Lorentz-Berthelot rules. TCNE^{•-} and NBu₄⁺ charges were fitted from the electrostatic potential (ESP) based on M06-L/6-31+G(d) calculations. The OPLS model^[51] was used for CH₂Cl₂ molecules. The 1-4 van der Waals and the 1-4 coulombic interactions were scaled down by a factor of 2.0. An atom based cutoff of 12 Å for non-bonded interactions was used and the long-range electrostatics were calculated using the PME (particle-particle mesh Ewald) summation method.^[52]

Table 1 collects the characteristics of the simulations performed herein. The MD simulations were carried out at 175 and 300 K starting with random velocities. Since the force field does not include explicit electronic effects (e.g. stabilizing orbital interactions), we used harmonic restraints to keep the dimer bound. The r_{\dots} distance between the

midpoints of the central C=C bonds was fixed at 2.732 Å with a harmonic potential of 50.0 kcal mol⁻¹ Å⁻². Furthermore, the near- D_{2h} symmetry was preserved through a restraint in the C=C \cdots C=C dihedral angles, with a harmonic potential of 50.0 kcal mol⁻¹ rad⁻². The temperature was tracked by coupling the system to a thermal bath using the Berendsen algorithm^[53] with a relaxation time of 1.0 ps. In the (NPT) simulations, the pressure was similarly coupled to a barostat^[53] with a relaxation time of 1.0 ps. A time step of 2 fs was used to integrate the equations of motion via the Verlet leapfrog algorithm.

The solutes were initially immersed in solution, taking as initial configuration their crystal geometry from the [NBu₄][TCNE] crystal (CCDC refcode IMEYEE), where π -[TCNE]₂²⁻ dimers are present. After 20,000 steps of energy minimization, 250 ps of dynamics were performed with fixed solutes (BELL option of AMBER) in order to allow solvent relaxation around the solute. This was followed by 250 ps of dynamics at constant volume and 500 ps of dynamics at constant temperature and at a constant pressure of 1 atm. Finally, the production run at constant volume and temperature (NVT) was performed. The coordinates were saved every 1 ps.

The change in the (Helmholtz) free energy profile for the dimerization process as a function of the TCNE^{•-} \cdots TCNE^{•-} distance r_{\dots} was decreased from 15.0 Å ($\lambda = 1$) to 3.0 Å ($\lambda = 0$) in regular intervals. The inverse association process was also performed to get information on the reliability of the obtained values. The computed free energies are Helmholtz free energies as simulations were performed in the NVT ensemble.

$$\Delta A = \int_0^1 \left\langle \frac{\partial H}{\partial \lambda} \right\rangle_\lambda d\lambda$$

The change in ΔA at each step λ was calculated by the thermodynamic integration method based on the equation above.^[54] The potential of mean force is obtained through the blue moon ensemble method.^[55,56] The transformation from the initial to the final state was achieved in 120 steps, i.e., with increments $\Delta\lambda$ corresponding to $\Delta r_{\dots} = 0.1$ Å. For each value of λ , 1260 ps equilibration + 2560 ps data times were employed at 175 K, while 160 + 320 ps collection times were employed at 300 K. The higher equilibration and data collection times at 175 K results from the slower diffusion at this temperature, compared to 300 K.

Ab initio MD (AIMD) simulations were performed using the Car–Parrinello scheme for propagating the

Table 1. Characteristics of the simulations carried out in the present work.

Solute	Solvent	Box Size (Å x Å x Å)	Time (ns)	T (K)
FFMD				
TCNE ^{•-} , NBu ₄ ⁺	464 CH ₂ Cl ₂	35.1 x 35.1 x 35.1	9	175
TCNE ^{•-} , NBu ₄ ⁺	464 CH ₂ Cl ₂	36.9 x 36.9 x 36.9	9	300
2 TCNE ^{•-} , 2 NBu ₄ ⁺	459 CH ₂ Cl ₂	35.2 x 35.2 x 35.2	100	175
2 TCNE ^{•-} , 2 NBu ₄ ⁺	459 CH ₂ Cl ₂	36.9 x 36.9 x 36.9	50	300
AIMD				
			(ps)	
2 TCNE ^{•-}	64 CH ₂ Cl ₂	18.3 x 18.3 x 18.3	46.3	175
2 TCNE ^{•-}	64 CH ₂ Cl ₂	19.2 x 19.2 x 19.2	52.3	300 ^a

^a The temperature was increased to 350 K during 18 ps in order to accelerate the dissociation process.

^b In its initial configuration, both NBu₄⁺ cations start ca. 16 Å away from the [TCNE]₂²⁻ dimer.

wavefunctions and the ionic configurations as implemented in the CPMD package.^[57] The PBE density functional^[58] was used for the electronic structure calculations, together with Vanderbilt pseudopotentials,^[59] and a wavefunction cutoff of 25 Ry. Empirical corrections introduced by Grimme to account for the van der Waals intermolecular interactions were used.^[60] The PBE-D2 density functional has been proven to accurately reproduce the long, multicenter bonding properties of π -[TCNE]₂²⁻ and π -[TTF]₂²⁺ dimers compared to high-level RASPT2 calculations.^[61] The time step was set to 4 a.u. and the fictitious mass for the orbitals was chosen to be 400 a.m.u. A cubic simulation box (of 18.331 Å side at 175 K and 19.165 Å side at 300 K) containing 64 CH₂Cl₂ molecules and one π -[TCNE]₂²⁻ dimer was used. Periodic boundary conditions were applied. The initial configurations were taken from equilibrated FFMD simulations. This was followed by a further equilibration of 2 ps in the canonical ensemble, in order to let the systems relax in the *ab initio* interaction potential. The Nosé-Hoover thermostat^[62-64] was used to get an average temperature of 175 or 300 K.

The free energy profile of the dissociation process at 175 K has been obtained from the AIMD, also by means of the thermodynamic integration method described above using the “dynamic distance” reaction coordinate.^[65] This coordinate r'_{\dots} is a mass-weighted root mean square of selected distances, here r_1 and r_2 (see Figure 1): $r'_{\dots} = (r_1^2 + r_2^2)^{1/2}$, where the mass term is neglected as all atoms involved are of the same type. This approach has been proven to be a versatile reaction coordinate for the study of processes involving the rupture and formation of a series of chemical bonds or contacts.^[65] The r'_{\dots} distance was stepwise increased from 2.25 Å to 10.0 Å using three different increment values ($\Delta r'_{\dots}$): $\Delta r'_{\dots} = 0.25$ Å from $r'_{\dots} = 2.25$ to $r'_{\dots} = 5.0$ Å, $\Delta r'_{\dots} = 0.50$ Å from 5.0 to 8.0 Å, and $\Delta r'_{\dots} = 1.0$ Å from 8.0 to 10.0 Å. The equilibration + data collection times, which vary for each r'_{\dots} distance, were always long enough to ensure convergence of the mean force.

Static QM DFT calculations were also carried out to support some of the AIMD results. They were performed with Gaussian 09,^[66] using the PBE-D2 density functional^[60] with the 6-31+G(d) basis set.^[67] The PCM approach, where the environment is modeled by a polarizable continuum medium, was used to model the dichloromethane solution ($\epsilon = 8.93$ for CH₂Cl₂).^[68,69] The free energy of dimerization and the activation free energy for the dissociation of the dimer were computed using vibrational frequencies obtained within the harmonic approximation.

Results and Discussion

The presentation of the results is organized as follows. We will first investigate by FFMD the distribution of NBu₄⁺ counterions around the TCNE⁻ monomer and its (TCNE)₂ dimer in DCM solution, in order to decipher whether the counterions play a crucial role in the stabilization of the dimer (section 1). Then, we shall examine by FFMD to which extent the solvation forces promote the “non-covalent” interaction of two TCNE⁻ anions, in the absence of

stabilizing electronic effects (section 2). After that, we will describe the structure and the stability of the π -dimers in DCM solution, taking into account electronic effects (AIMD results in section 3). Finally, we will reveal the structure of the solvation shell around the π -[TCNE]₂²⁻ dimer (section 4).

1. Ion pairing in dichloromethane solution: FFMD simulations on the (NBu₄⁺)(TCNE⁻) single ion pair and the (NBu₄⁺)₂(TCNE)₂ aggregate.

In order to understand the behavior of NBu₄⁺ and TCNE⁻ in solution, we first simulated by FFMD the single (NBu₄⁺)(TCNE⁻) ion pair, starting with the ions in contact (run details are collected in Table 1 and the initial configuration is shown in Figure S1). During the dynamics, at both 175 K and 300 K, the ion pair dissociates (Figure 2), showing a high diffusion of both ions along the simulation box, with transient close contacts. Therefore, NBu₄⁺ and TCNE⁻ ions are well solvated enough by DCM to overcome the coulombic attraction that would keep them paired together.

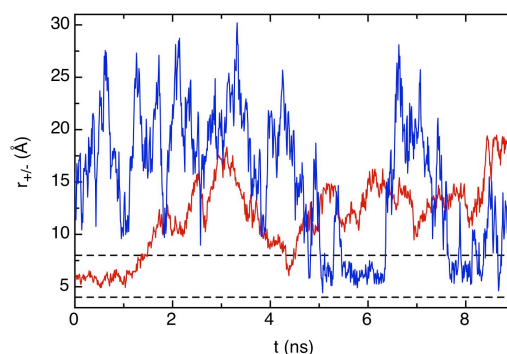


Figure 2. Time-resolved evolution of the interionic distance $r_{+,-}$ (Å) between a TCNE⁻ ion and a NBu₄⁺ as obtained from FFMD simulations of an (TCNE⁻)(NBu₄⁺) ion pair in CH₂Cl₂, at 175 K (red curve) and 300 K (blue curve). The $r_{+,-}$ distance was defined as the distance between the midpoint of the central C=C atoms of the TCNE and the N atom of the cation. The dashed lines delineate the region for a contact ion pair.

FFMD simulations were then carried out on the (NBu₄⁺)₂(TCNE)₂ aggregate at 175 and 300 K (details shown in Table 1). When the [TCNE]₂²⁻ dimer was free of constraints it was observed that it spontaneously dissociates at both 175 and 300 K (see Figure S3). In order to investigate the status of counterions around the π -dimer in the conditions where it forms, i.e. at 175 K, we thus constrained the latter to its *D*_{2h} structure (see the Methodological details section) and performed a long FFMD run (100 ns) in order to sample enough different states. The position of the cations was monitored via their distances with respect to the center of mass of the dimer, along the whole trajectory (see Figure 3). Starting from a configuration in which the two NBu₄⁺ ions are in contact with the π -dimer (Figure S2), one of the counterions dissociates and diffuses into the bulk solution very early. Subsequently, the simulations reveal several exchange processes, whereby a given cation gets closer to the π -dimer, form a short contact with it and then moves away. Ion pairing in DCM solution is thus a dynamic process. Overall, during only ca. 25% of the time, is one of the

counterions in contact with the dimer. Besides, the two NBu_4^+ ions were never observed to be simultaneously in contact with the $[\text{TCNE}]_2^{2-}$ dimer along the simulations. Therefore, cations should have no significant contribution to the stability of the dimer in DCM solution, in good agreement with the experimental results.^[8] Finally, it is worth mentioning that ion-pairing is expected to play a more important role in less polar solvents, like chloroform (see Figure S4).

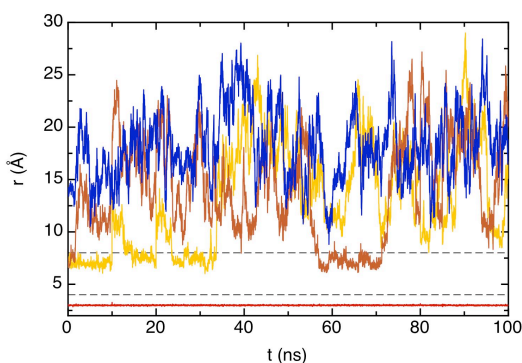


Figure 3. FFMD simulation of the constrained π -dimer in dichloromethane at 175 K, starting with paired NBu_4^+ counterions. Distances (\AA) as a function of time (ns): $\text{TCNE}\cdots\text{TCNE}$ in red ($r_{c,c}$), $\text{NBu}_4^+\cdots\text{NBu}_4^+$ in blue ($r_{+,+}$), and $(\text{TCNE})_2^{2-}\cdots\text{NBu}_4^+$ distances in orange and brown ($r_{+,c}$). The dashed lines delineate the region for a contact $(\text{TCNE})_2^{2-}\cdots\text{NBu}_4^+$ ion pair.

2. Interactions between two TCNE^- anions in dichloromethane solution, investigated by PMF FFMD simulations.

In this section, we shall determine the interaction between two TCNE^- anions in DCM solution in the absence of the SOMO-SOMO overlap component, that is to say, we shall evaluate the effective “non-covalent” interaction between these ions. It is indeed crucial to assess to which extent the two anions repulse each other before the stabilizing intermolecular orbital overlap (and thus the electron pairing) becomes important. The large coulombic repulsion between two TCNE^- ions separated 3 \AA in DCM solution (whose dielectric constant is 8.9) should in principle prevent the formation of stable stacked “non-covalent” dimers. There are however cases where, due to solvation forces, two like-charged planar ions can “attract each other” and form π -stacked dimers, without requiring specific orbital interactions (see e.g. the case of the (picrate) $_2^{2-}$ or (guanidinium) $_2^{2+}$ dimers in water).^[43–49] In order to investigate whether, in the absence of orbital interactions, the two TCNE^- ions repulse or even “attract” each other in DCM solution, we decided to calculate by FFMD PMF simulations the change in free energy $\Delta A(r_{c,c})$ as a function of the distance $r_{c,c}$ between the two TCNE^- anions, in the presence of NBu_4^+ counterions (in Figure S5 we provide evidence that the sampling used to obtain the $\Delta A(r_{c,c})$ curves is sufficient).

As shown in Figure 4, a metastable minimum is found in the free energy profile obtained at 175 K, with a barrier toward dissociation of $\approx 0.8 \text{ kcal mol}^{-1}$ at $r_{c,c} \approx 4.5 \text{ \AA}$. On the contrary, no minimum is found

for the bound dimer at the higher temperature. Owing to the neglect of stabilizing orbital interactions in these FFMD simulations, the stability of the dimer is certainly underestimated. The results are however very important because they bring to light that, in solution, two TCNE^- anions can approach each other up to distances as short as 4 \AA at a modest energy cost (only ca. 1 kcal mol^{-1} at 175 K and $3.5 \text{ kcal mol}^{-1}$ at 300 K), in spite of their strong mutual repulsion (which amounts to 53 kcal mol^{-1} , according to the energy decomposition analysis along the FFMD trajectories).

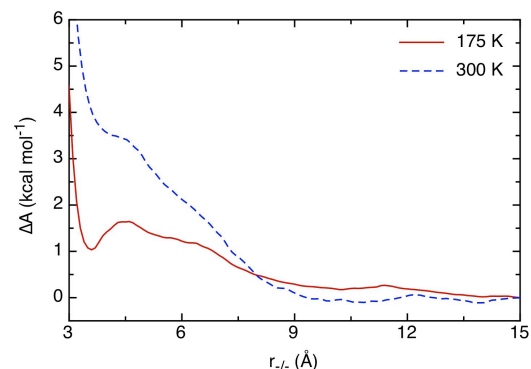


Figure 4. FFMD free energy profiles of the $(\text{TCNE})_2^{2-}$ dissociation process at 175 K and 300 K in DCM solution, in the presence of NBu_4^+ counterions. $r_{c,c}$ is the distance between the midpoints of the $\text{C}=\text{C}$ bonds of each TCNE^- .

Visualization of the trajectories along the PMF confirms that the NBu_4^+ counterions do not pair with the anions, and that all ions are mainly surrounded by CH_2Cl_2 solvent molecules (Figure S6). The lessened repulsion between TCNE^- anions at short distances are thus mainly caused by solvation effects: the $(\text{TCNE})_2^{2-}$ dianion is much better solvated than are the two separated anions. This feature is evidenced by an energy component analysis along the PMF (see Figure S7): when the $r_{c,c}$ separation is diminished from 15.0 to 3.6 \AA , the increase in $\text{TCNE}^- \cdots \text{TCNE}^-$ repulsion ($28 \pm 1 \text{ kcal mol}^{-1}$) is found to be more than compensated by the gain in $(\text{TCNE})_2^{2-} \cdots \text{solvent}$ attraction energy ($-88 \pm 7 \text{ kcal mol}^{-1}$), while the change in intra-solvent energy is small ($-10 \pm 14 \text{ kcal mol}^{-1}$) at either 175 K or 300 K. The peculiar solvation structure of the dimer will be analyzed in section 4.

3. Structure and stability of the π - $[\text{TCNE}]_2^{2-}$ dimer in solution, investigated by AIMD simulations.

We now turn to the AIMD results, based on a QM-DFT representation of the potential energy of the whole system, explicitly including its electronic structure. First, the π - $[\text{TCNE}]_2^{2-}$ dimer has been simulated unconstrained in order to explore its structure and stability at 175 and 300 K in DCM solution (see Table 1 for further details). No explicit cations have been introduced in the simulations because we demonstrated in the previous section that they are not crucial in the stabilization of the π -dimer. When simulated for 46.3 ps at 175 K in solution, the dimer remains associated and fluctuates around its D_{2h} -like geometry, featuring a cofacial arrangement of the radicals at an interplanar separation of 2.9 \AA

(see Figure S8). Furthermore, the TCNEs in the dimer are not planar, as their $\text{C}(\text{CN})_2$ moieties are tilted away from the plane of the adjacent $\text{C}=\text{C}$ bond (see the inset in Figure 6).

The $\text{TCNE}\cdots\text{TCNE}$ distance r_{\perp} has been also tracked at higher temperature, for a total duration of 52.3 ps (Figure 5). During a first sequence of 12 ps at 300 K, the dimer remains bound ($r_{\perp} \approx 3.0$ Å). The temperature was then increased to 350 K during 18 ps (shown between dashed lines in Figure 5) to promote the dissociation process. Indeed, after 6 ps at 350 K, the dimer starts dissociating, and is fully dissociated after 18 ps ($r_{\perp} \approx 9$ –10 Å). The temperature was then reset to 300 K and the dimer remained dissociated. Although the simulated AIMD timescales are limited by computational costs, we note that the AIMD results are consistent with the experimental observation that the dimers do not form at room temperature^[8,37]

Let us now examine the AIMD free energy profiles at 175 K for the dissociation process in DCM solution (Figure 6), and in the gas phase for comparison (Figure S9). In solution, the $\Delta A(r'_{\perp})$ curve exhibits a stable minimum at around 3.0 Å, with a barrier toward dissociation of 9.6 kcal mol⁻¹. It should be mentioned that the large barrier toward dissociation found in our AIMD simulations is in line with the results reported in Ref. [41], where the stability of the $(\text{TCNE})_2^{2-}$ dimer in solution was assessed for the first time by means of PCM-based static calculations (using PCM-tetrahydrofuran environment). Our simulations also show that the dimer's formation is favorable at 175 K, by $\Delta A = -5.5$ kcal mol⁻¹, in qualitative agreement with the experiments.^[8] On the contrary, static calculations (performed with G09 at PBE-D2/6-31+G(d) level using PCM-dichloromethane environment) predict a metastable minimum at 2.90 Å, with a ΔA (175 K) = 3.6 kcal mol⁻¹ and a barrier toward dissociation of 7.1 kcal mol⁻¹. Hence, the stable nature of the dimer is properly reproduced by the AIMD results with explicit solvent, but not with the static calculations with implicit solvent, hinting for specific solvation patterns. In stark contrast with the scenario found in solution, the AIMD free energy profile computed in the gas phase (Figure S9) demonstrates that the π -dimer cannot form in the gas phase due to its large instability with respect to dissociation and its vanishingly small barrier toward dissociation (0.8 kcal mol⁻¹).

Finally, the AIMD free energy profile at 175 K offers valuable insight into the mechanism of dissociation/formation of the π -dimer in solution. As shown in the snapshots of Figure 8 and by the time evolution of the r_1 and r_2 distances (Figure S10), the dissociation of the dimer at its early stages (up to a r distance of ca. 4.0 Å) follows a concerted mechanism, which preserves the D_{2h} symmetry on the average. This feature is in keeping with the π -orbital overlap between the anions. On the other hand, for r'_{\perp} values higher than 4.2 Å the dissociation process switches to a "stepwise mechanism", whereby one of the r_1 and r_2 distances is always larger than the other distance. It is worth mentioning that a very similar dissociation mechanism is observed in the unconstrained AIMD simulation at 300–350 K.

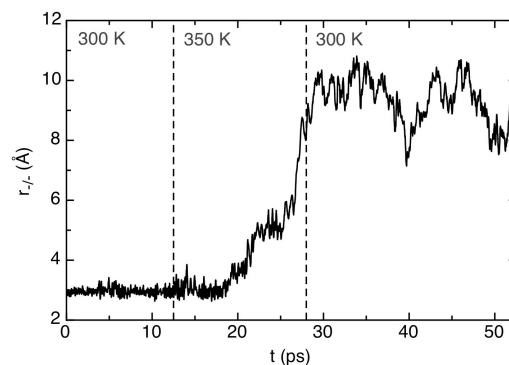


Figure 5. Time evolution of the $\text{TCNE}\cdots\text{TCNE}$ distance, at 300 K. The temperature was raised to 350 K during the 18 ps comprised between the two dashed lines in order to accelerate the dissociation process.

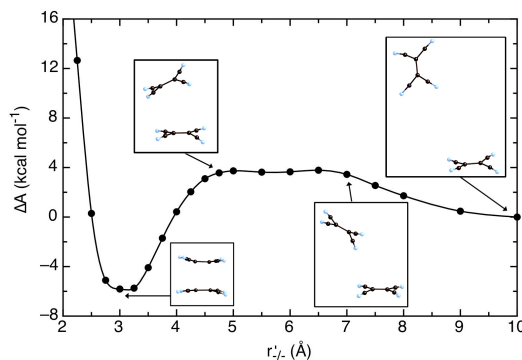


Figure 6. AIMD free energy profiles of the π - $[\text{TCNE}]_2^{2-}$ dissociation process at 175 K in DCM solution. r'_{\perp} is the intermonomer dynamic-distance reaction coordinate (see text). Representative snapshots along the reaction coordinate are shown as insets, where the solvent molecules are not shown for a better view.

4. Structure of the first solvation shell of the π - $[\text{TCNE}]_2^{2-}$ dimer in dichloromethane solution.

In the previous section we concluded that the π - $[\text{TCNE}]_2^{2-}$ dimer preserves the D_{2h} -like structure during the whole simulation at 175 K and that it is thermodynamically stable. The analysis of its first solvation shell obtained from the AIMD trajectories will demonstrate that this stability is a direct consequence of specific π - $[\text{TCNE}]_2^{2-}\cdots$ solvent interactions.

We first focus on the radial distribution function (RDF) between the carbon atoms of the dichloromethane molecules (C_{DCM}) and the center of mass of the dimer (bottom graphic of Figure 7). This RDF displays a broad peak ranging from 4.0 Å up to 7.3 Å, with two components. The integration up to 7.3 Å provides a coordination number of 20 CH_2Cl_2 molecules. As shown in Figure 8, where a representative configuration of the first solvation shell is displayed, these twenty CH_2Cl_2 molecules split into two sub-groups, of eight + twelve molecules, respectively: eight are located in the "equatorial" plane (bisecting the two TCNE planes) and the twelve others (depicted in light green color in Figure 8) are located below and above the π -dimer, leaving a depleted region with conical shape that forms an angle of $\sim 20^\circ$ with the "vertical" axis.

Among the eight equatorial solvent molecules, two sit in positions of type 1, four in positions of type 2, and two in positions of type 3 (see Figure 9 for

labeling). These positions are in fact close to minimum energy configurations in the potential energy surface of a single CH_2Cl_2 molecule interacting with a π -dimer (Figure 9). According to QM static calculations in the gas phase, the most favorable position is of type **1** (where the interaction energy between CH_2Cl_2 and the π -dimer is $-15.2 \text{ kcal mol}^{-1}$), closely followed by positions **2** and **3** (by $\Delta E = 0.1$ and $1.5 \text{ kcal mol}^{-1}$, respectively). In these three optimized positions, CH_2Cl_2 connects the two TCNE moieties via different bridging H-bonding interactions with the N-atoms. In positions **1** and **3**, each H_{DCM} atom interacts with two N-atoms belonging to different TCNEs, while in position **2**, each H_{DCM} interacts with a single N-atom. As a result, the $\text{H}_{\text{DCM}}\cdots\text{N}$ intermolecular bonds are somewhat shorter in **2** than in **1** or **3** positions (see Figure 9). At this point, it should be noticed that optimal interaction energies between the dimer and an equatorial CH_2Cl_2 molecule are substantially larger than the interaction energy between CH_2Cl_2 and a TCNE \cdot monomer, which is $-10.1 \text{ kcal mol}^{-1}$. This explains why in DCM solution the π -dimer is much better solvated than are the constituent monomers (cf. analysis of PMF results in section 2).

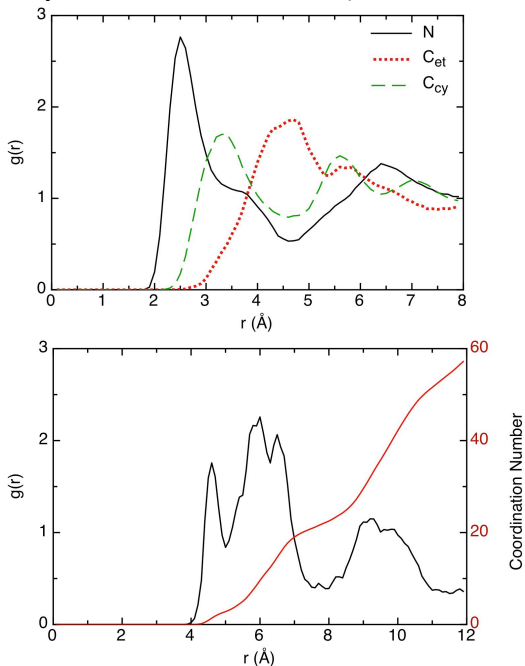


Figure 7. (top) RDF of H_{DCM} atoms around each TCNE atom type at 175 K. (bottom) RDF of C_{DCM} atoms around the center of mass of the $[\text{TCNE}]_2^{2-}$ dimer at 175 K (black curve) and the associated coordination number (red curve). Both RDFs were obtained from the AIMD simulations.

During the whole dynamics in solution, the eight equatorial molecules stay within the first solvation shell. The two ones sitting in positions **1** are the most tightly bound to the π -dimer. This is evidenced in Figures 10 and S11, where each of their H_{DCM} atoms makes a $\text{H}_{\text{DCM}}\cdots\text{N}$ short contact (ca. 2.4 \AA) during almost the whole simulation. The CH_2Cl_2 molecules in positions **2**, in turn, are more loosely bound, as they display only one short $\text{H}_{\text{DCM}}\cdots\text{N}$ contact, sometimes switching the interacting hydrogen (Figures 10 and S11). Concerning the two CH_2Cl_2

molecules in positions **3**, one is tightly bound to the π -dimer (as in position **1**), while the other one is more labile (as in position **2**).

The twelve other CH_2Cl_2 molecules of the first solvation shell sit above and below the π -dimer, and also make short $\text{C-H}\cdots\text{N}$ contacts during the whole simulation. However, these are more labile than those exhibited by the equatorial molecules (see Figure S12). Indeed, a CH_2Cl_2 molecule sitting on top of the π -dimer interacts with the latter less than does an equatorial CH_2Cl_2 molecule (by ca. 5 kcal mol^{-1} , according to the QM energy minimizations).

To complete our analysis in terms of H-bonding interactions, we now turn to the RDFs between H_{DCM} atoms and the three atoms types of TCNE (that is, N, C_{cy} , and C_{et} ; see Figure 1). As displayed in the top graphic of Figure 7, the RDF around the eight N atoms exhibits a maximum at $2.4\text{--}2.6 \text{ \AA}$, while around the eight C_{cy} and the four C_{et} the RDF peaks are centered at $3.2\text{--}3.4 \text{ \AA}$ and $4.25\text{--}4.75 \text{ \AA}$, respectively. Given the nature of the $\text{C-H}\cdots\text{A}$ hydrogen bonds (where A is a Lewis donor), which typically have a length of around 2.4 \AA ,^[70] we can conclude that the H-bonds between the π -dimer and the solvent are mainly of $\text{C-H}\cdots\text{N}$ type. The integration of the $\text{H}_{\text{DCM}}\cdots\text{N}$ RDF (up to 3.3 \AA) provides a coordination number of 4 hydrogens around each N-atom. Among these hydrogens, three belong to equatorial CH_2Cl_2 molecules, and only one belongs to molecules in other positions. It thus follows that the $\text{C-H}\cdots\text{N}$ interactions arising from the eight equatorial CH_2Cl_2 molecules afford the main stabilizing interactions of the dimer in solution. A detailed analysis of the different contributions is given in Figure S13. The conical depleted regions at the top and at the bottom of the dimer (see Figure 8) correspond in fact to CH_2Cl_2 molecules that are not H-bonded to N-atoms of the dimer.

Interestingly, the FFMD trajectories exhibit similar solvation patterns as the AIMD ones. The first shell involves 18 CH_2Cl_2 molecules (see Figure S14). Among them, about eight also sit in equatorial positions. We note that, in the force field model used for the FFMD simulations, the H_{DCM} atoms are not explicitly represented, but implicitly within the united atom approximation (i.e. via a bigger C atom). This feature indicates that the stabilization of the dimer by CH_2Cl_2 molecules mainly stems from charge-dipole electrostatic interactions. These are indeed the main energy contributions to H-bonds^[71] and should also operate in polar solvents like acetone or alkyl-nitriles where the π - $[\text{TCNE}]_2^{2-}$ dimer has been detected.^[8] They should likewise stabilize dicationic π -dimers like $[\text{OMB}]_2^{2+}$ ($\text{OMB}\cdot^+$ is the octamethylbiphenylene radical cation) in DCM solution where the CH_2Cl_2 hydrogens cannot be H-bonded to the dimer.^[8] On the thermodynamic side, we note that “freezing” such solvent molecules around the dimer likely contributes to the unfavorable entropy of dimerization in solution.^[8]

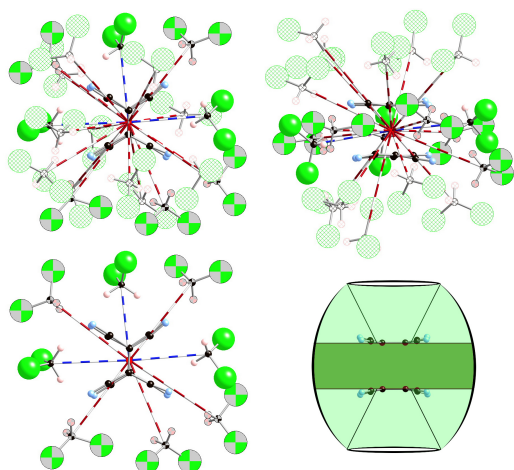


Figure 8. Top and side views of the first solvation shell of π -[TCNE] $_2^{2-}$ (top). The eight “equatorial” CH_2Cl_2 molecules that contribute most to the dimer stabilization are shown highlighted, and this region is marked in dark green in the scheme (bottom). The three equatorial molecules that are most tightly bound are connected to the dimer’s center of mass with dashed blue lines, while the other five equatorial molecules are depicted in flat green-grey.

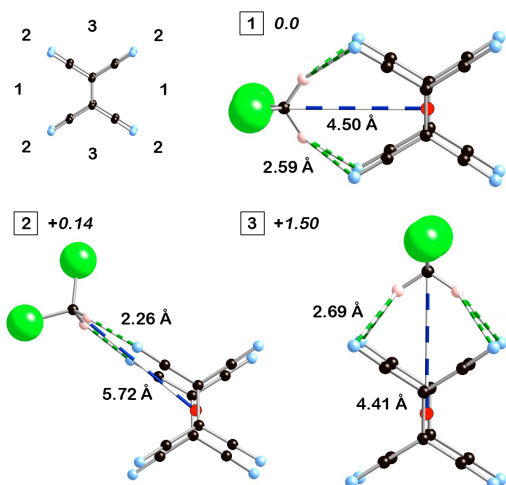


Figure 9. The three most stable positions of a CH_2Cl_2 molecule around the dimer, obtained from static DFT optimizations at the PBE-D2/6-31+G(d) level. The relative energies, ΔE in kcal mol^{-1} , are given in italics.

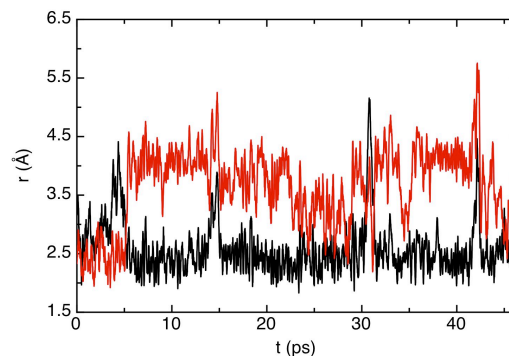
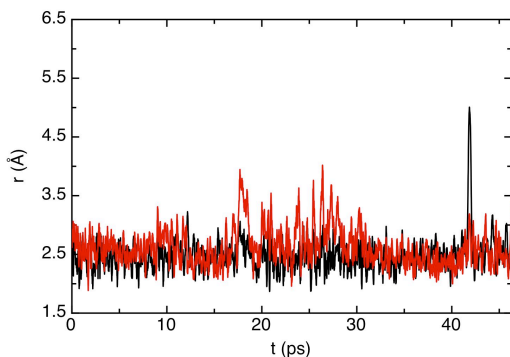


Figure 10. Time evolution of the shortest $\text{H}_{\text{DCM}}\cdots\text{N}$ distance for each H-atom of a CH_2Cl_2 molecule sitting in equatorial positions **1** (top) or **2** (bottom). The molecule in the other position **1** behaves as the one depicted here (see Figure S11). The three other molecules in positions **2** behave as the one depicted in the bottom panel (Figure S11). Concerning the two CH_2Cl_2 molecules in positions **3**, one follows the top behavior whereas the other features the bottom behavior.

Conclusions

The solvation and stability of the π -[TCNE] $_2^{2-}$ dimer has been exhaustively studied by means of MD and free energy PMF simulations in the explicitly represented condensed phase for the first time, thereby furnishing the most realistic description of long, multicenter π -dimers in solution so far reported. This study has been conducted using two complementary representations of the potential energy. On the one hand, features stemming from “non-covalent” interactions have been investigated at the multisecond timescale by means of FFMD simulations. On the other hand, those aspects involving explicitly represented electronic effects have been examined at the multipicosecond timescale by means of AIMD simulations.

FFMD simulations have demonstrated that $(\text{NBU}_4^+)_2[\text{TCNE}]_2^{2-}$ aggregates, with two NBU_4^+ ions in permanent contact with the π -[TCNE] $_2^{2-}$ dimer, do not form in dichloromethane solution. Although ion-pairs comprising a π -dimer and one NBU_4^+ ion do form intermittently, the π -dimer is fully solvated by DCM molecules most of the time (ca. 75% of the simulation time). It thus follows that counterions do not play any essential role in stabilizing π -[TCNE] $_2^{2-}$ dimers in DCM solution.

AIMD simulations on the π -[TCNE] $_2^{2-}$ dimer in dichloromethane at 175 K have provided the definitive proof that π -dimers of long-bonded ionic radicals are stable in solution at low temperatures. The structure of the TCNE $^{\cdot-}$ dimers in solution is almost identical to that found in crystals, i.e., they feature a cofacial arrangement of the radicals with D_{2h} symmetry and an interplanar separation of 3 Å. The free energy profile for the π -dimer dissociation extracted from the AIMD simulations at 175 K provides a stable dimer by $-5.5 \text{ kcal mol}^{-1}$ and a barrier toward dissociation of $9.6 \text{ kcal mol}^{-1}$. In contrast with the low-temperature scenario, AIMD simulations conducted at 300–350 K have shown that the π -dimers are not stable. The AIMD simulations have also shed light on the mechanism of

dissociation/formation of the π -dimers. Up to interplanar distances of about 4 Å, the dissociation follows a concerted mechanism, whereby the interfragment distances between central carbon atoms increase in a synchronous fashion. For interplanar distances larger than ~4 Å, in turn, the dissociation follows a stepwise mechanism, whereby one of the interfragment distances between central carbon atoms is always larger than the other one, thus breaking the D_{2h} symmetry of the dimer.

The stability of the π -[TCNE] $_2^{2-}$ dimer in DCM solution originates in the fact that the dimer is much better solvated than are the corresponding monomers. The AIMD simulations conducted at 175 K have revealed a unique solvation structure around the π -dimer. Among the twenty CH₂Cl₂ molecules in the first solvation shell, eight sit in the equatorial plane of the “barrel-shaped” dimer and afford the main stabilizing interactions in solution. They sit near the eight positions intrinsically preferred (in the gas phase) where they “glue” the two TCNE moieties together via strong bridging CH \cdots N hydrogen bonds. The better solvation of the π -[TCNE] $_2^{2-}$ dimer (compared to that of the monomers) also explains why the two like-charged monomers can approach each other in DCM solution without significant energy penalty before the stabilizing intermolecular orbital overlap sets in.

The strong attractive interactions between DCM molecules and the π -[TCNE] $_2^{2-}$ dimer, and thus the stabilization of this π -dimer in DCM solution, mainly arise from charge-dipole electrostatic interactions. The herein unveiled key role of charge-dipole electrostatic interactions in promoting the formation of π -[TCNE] $_2^{2-}$ dimers in DCM solution is not only a relevant finding for the system herein studied, but also crucial to rationalize ion-pairing of TCNE $^-$ anions in other solvents and ion-pairing of other charged radicals. Indeed, the same kind of electrostatic interactions are expected to explain the formation of π -[TCNE] $_2^{2-}$ dimers in other polar solvents, such as acetone and alkyl-nitriles.^[8] Electrostatic interactions are also expected to be the key factor behind the stability of π -dimers of charged radicals that cannot form hydrogen bonds with solvent molecules (for instance, the π -dimer of the octamethylbiphenylene radical cation in DCM).

The in-depth knowledge on the structure and the peculiar solvation shell of π -[TCNE] $_2^{2-}$ dimers in dichloromethane provided by our study, together with the demonstration of the prime role played by solvation forces of a polar organic solvent in stabilizing these dimers, constitute a milestone toward achieving a full understanding of the intriguing phenomenon of pairing of like-charged organic radicals in solution. The results herein presented are relevant in the context of crystal engineering (the formation of crystals containing π -dimers should in principle be favored if the solution from which the crystals are grown contains dimers) and molecular switching applications in view of the increasing use of ionic radicals as building blocks for functional molecular materials and supramolecular aggregates.

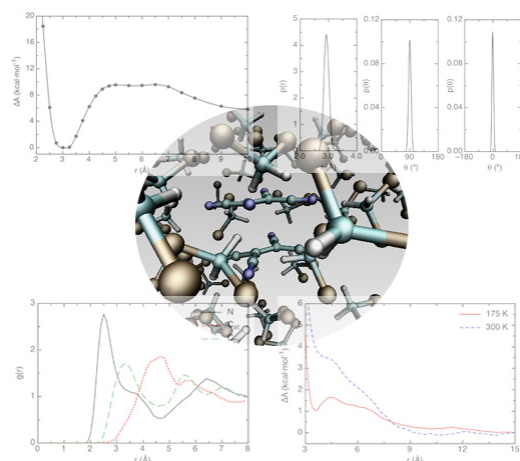
Supporting Information

Supporting information for this article is available on the WWW. This contains: Initial configuration of the (NBu₄⁺)(TCNE⁻) single ion pair in FFMD simulations of Figure 1; Initial configuration of the (NBu₄⁺)₂(TCNE⁻)₂ aggregate in FFMD simulations of Figure 2; Initial configuration of the (NBu₄⁺)(TCNE⁻)₂ aggregate in FFMD simulations of Figure 3; Distances as a function of time on the (TCNE⁻)₂(NBu₄⁺)₂ aggregate in chloroform at 175 K, starting from remote initial geometry; Snapshots of (TCNE⁻)₂(NBu₄⁺)₂ aggregate along the PMF of the dissociation process (Figure 4) at 175 K in dichloromethane. Free energy profile at 175 K obtained in the gas phase; RDF of the solvent molecules around the dimer obtained from the FFMD; Distance plots for several values of dynamic distance of the AIMD dissociation profile; PDFs of the H_{DCM \cdots N} distance of both hydrogens of each CH₂Cl₂ molecule within the closest solvation shell; Time evolution of the distance between both hydrogen atoms of each CH₂Cl₂ molecule of positions **1**, **2**, and **3** with their closest N; Time evolution of the distance between both hydrogen atoms of each CH₂Cl₂ molecule within the first solvation shell with their closest N.

Acknowledgements

M.C.-C., J.R.-A., and J.J.N. acknowledge the MINECO of Spain (MAT2011-25972, MAT2014-54025-P), Generalitat de Catalunya (2014-SGR-1422), CSUC and BSC. M.C.-C. gratefully acknowledges the Spanish Government for a “Juan de la Cierva – Formación” fellowship. A.C. and W.G. thank IDRIS, CINES, and UdS for computational support. We would also like to thank Prof. Nikos Doltsinis for kindly providing us with the CPMD subroutine of the “dynamic distance” reaction coordinate.

Table of Contents



References

- [1] J. S. Miller, J. J. Novoa, *Acc. Chem. Res.* **2007**, *40*, 189–196.
- [2] K. E. Preuss, *Polyhedron* **2014**, *79*, 1–15.
- [3] R. Chang, *J. Phys. Chem.* **1970**, *74*, 2029–2030.
- [4] M. Itoh, *Bull. Chem. Soc. Jpn.* **1972**, *45*,

- 1947–1950.
- [5] J. J. Novoa, P. Lafuente, R. E. Del Sesto, J. S. Miller, *Angew. Chem. Int. Ed.* **2001**, *40*, 2540–2545.
- [6] R. E. Del Sesto, J. S. Miller, P. Lafuente, J. J. Novoa, *Chem. - Eur. J.* **2002**, *8*, 4894–4908.
- [7] J. J. Novoa, P. Lafuente, R. E. Del Sesto, J. S. Miller, *CrystEngComm* **2002**, *4*, 373–377.
- [8] J.-M. Lü, S. V. Rosokha, J. K. Kochi, *J. Am. Chem. Soc.* **2003**, *125*, 12161–12171.
- [9] A. A. Trifonov, I. D. Gudilenkov, G. K. Fukin, A. V. Cherkasov, *Organometallics* **2009**, *28*, 3421–3425.
- [10] S. Z. Goldberg, B. Spivack, G. Stanley, R. Eisenberg, D. M. Braitsch, J. S. Miller, M. Abkowitz, *J. Am. Chem. Soc.* **1977**, *99*, 110–117.
- [11] C. Willi, A. H. Reis, E. Gebert, J. S. Miller, *Inorg. Chem.* **1981**, *20*, 313–318.
- [12] J. Huang, S. Kingsbury, M. Kertesz, *Phys. Chem. Chem. Phys.* **2008**, *10*, 2625–2635.
- [13] R. C. Teitelbaum, T. J. Marks, C. K. Johnson, *J. Am. Chem. Soc.* **1980**, *102*, 2986–2989.
- [14] J. Morgado, I. C. Santos, L. F. Veiros, C. Rodrigues, R. T. Henriques, M. T. Duarte, L. Alcácer, M. Almeida, *J. Mater. Chem.* **2001**, *11*, 2108–2117.
- [15] K. Goto, T. Kubo, K. Yamamoto, K. Nakasuji, K. Sato, D. Shiomi, T. Takui, M. Kubota, T. Kobayashi, K. Yakusi, et al., *J. Am. Chem. Soc.* **1999**, *121*, 1619–1620.
- [16] D. Small, V. Zaitsev, Y. Jung, S. V. Rosokha, M. Head-Gordon, J. K. Kochi, *J. Am. Chem. Soc.* **2004**, *126*, 13850–13858.
- [17] M. Capdevila-Cortada, J. J. Novoa, J. D. Bell, C. E. Moore, A. L. Rheingold, J. S. Miller, *Chem. - Eur. J.* **2011**, *17*, 9326–9341.
- [18] J. S. Miller, A. J. Epstein, *Angew. Chem. Int. Ed.* **1994**, *33*, 385–415.
- [19] J. R. Ferraro, J. M. Williams, *Introduction to Synthetic Electrical Conductors*, Academic Press, Orlando, **1987**.
- [20] T. Ishiguro, K. Yamaji, G. Saito, *Organic Superconductors*, Springer, New York, **1998**.
- [21] J. S. Miller, *Angew. Chem. Int. Ed.* **2006**, *45*, 2508–2525.
- [22] E. B. Vickers, T. D. Selby, M. S. Thorum, M. L. Taliaferro, J. S. Miller, *Inorg. Chem.* **2004**, *43*, 6414–20.
- [23] E. B. Vickers, T. D. Selby, J. S. Miller, *J. Am. Chem. Soc.* **2004**, *126*, 3716–7.
- [24] H. Okamoto, K. Ikegami, T. Wakabayashi, Y. Ishige, J. Togo, H. Kishida, H. Matsuzaki, *Phys. Rev. Lett.* **2006**, *96*, 037405.
- [25] J. M. Spruell, A. Coskun, D. C. Friedman, R. S. Forgan, A. A. Sarjeant, A. Trabolsi, A. C. Fahrenbach, G. Barin, W. F. Paxton, S. K. Dey, et al., *Nat. Chem.* **2010**, *2*, 870–879.
- [26] M. Capdevila-Cortada, J. J. Novoa, *Chem. - Eur. J.* **2012**, *18*, 5335–5344.
- [27] P.-T. Chiang, N.-C. Chen, C.-C. Lai, S.-H. Chiu, *Chem. - Eur. J.* **2008**, *14*, 6546–6552.
- [28] M. Fumanal, M. Capdevila-Cortada, J. S. Miller, J. J. Novoa, *J. Am. Chem. Soc.* **2013**, *135*, 13814–13826.
- [29] A. Y. Ziganshina, Y. H. Ko, W. S. Jeon, K. Kim, *Chem. Commun.* **2004**, 806–807.
- [30] M. Capdevila-Cortada, J. S. Miller, J. J. Novoa, *Chem. - Eur. J.* **2014**, *20*, 7784–95.
- [31] J. M. Spruell, *Pure Appl. Chem.* **2010**, *82*, 2281–2294.
- [32] F. Mota, J. S. Miller, J. J. Novoa, *J. Am. Chem. Soc.* **2009**, *131*, 7699–7707.
- [33] Z.-H. Cui, H. Lischka, T. Mueller, F. Plasser, M. Kertesz, *Chemphyschem* **2014**, *15*, 165–176.
- [34] M. Capdevila-Cortada, J. S. Miller, J. J. Novoa, *Chem. - Eur. J.* **2015**, *21*, 6420–6432.
- [35] I. Garcia-Yoldi, F. Mota, J. J. Novoa, *J. Comput. Chem.* **2006**, *28*, 326–334.
- [36] Y. Jung, M. Head-gordon, *Phys. Chem. Chem. Phys.* **2004**, *6*, 2008–2011.
- [37] S. V. Rosokha, J. K. Kochi, *J. Am. Chem. Soc.* **2007**, *129*, 828–838.
- [38] I. Garcia-Yoldi, J. S. Miller, J. J. Novoa, *J. Phys. Chem. A* **2007**, *111*, 8020–8027.
- [39] I. Garcia-Yoldi, J. S. Miller, J. J. Novoa, *J. Phys. Chem. A* **2009**, *113*, 7124–7132.
- [40] I. Garcia-Yoldi, J. S. Miller, J. J. Novoa, *J. Phys. Chem. A* **2009**, *113*, 484–492.
- [41] J. Jakowski, J. Simons, *J. Am. Chem. Soc.* **2003**, *125*, 16089–16096.
- [42] Q. Wang, M. D. Newton, *J. Phys. Chem. B* **2008**, *112*, 568–576.
- [43] S. Boudon, G. Wipff, B. Maigret, *J. Phys. Chem.* **1990**, *94*, 6056–6061.
- [44] K. T. No, K.-Y. Nam, H. A. Scheraga, *J. Am. Chem. Soc.* **1997**, *119*, 12917–12922.
- [45] L. Troxler, J. M. Harrowfield, G. Wipff, *J. Phys. Chem. A* **1998**, *102*, 6821–6830.
- [46] P. E. Mason, G. W. Neilson, J. E. Enderby, M.-L. Saboungi, C. E. Dempsey, A. D. MacKerell, J. W. Brady, *J. Am. Chem. Soc.* **2004**, *126*, 11462–70.
- [47] M. Vazdar, F. Uhlig, P. Jungwirth, *J. Phys. Chem. Lett.* **2012**, *3*, 2021–2024.
- [48] T. Inagaki, S. Aono, H. Nakano, T. Yamamoto, *J. Phys. Chem. B* **2014**, *118*, 5499–508.
- [49] D. Bandyopadhyay, K. Bhanja, S. Mohan, S. K. Ghosh, N. Choudhury, *J. Phys. Chem. B* **2015**, *119*, 11262–74.
- [50] D. A. Case, T. A. Darden, T. E. Cheatham III, C. L. Simmerling, J. Wang, R. E. Duke, R. Luo, M. Crowley, R. C. Walker, W. Zhang, et al., AMBER 10, University of California, San Francisco.
- [51] W. L. Jorgensen, J. M. Briggs, M. L. Contreras, *J. Phys. Chem.* **1990**, *94*, 1683–1686.
- [52] T. Darden, D. York, L. Pedersen, *J. Chem. Phys.* **1993**, *98*, 10089.
- [53] H. J. C. Berendsen, J. P. M. Postma, W. F. van Gunsteren, A. DiNola, J. R. Haak, *J. Chem. Phys.* **1984**, *81*, 3684.
- [54] P. Kollman, *Chem. Rev.* **1993**, *93*, 2395–2417.
- [55] E. A. Carter, G. Ciccotti, J. T. Hynes, R. Kapral, *Chem. Phys. Lett.* **1989**, *156*, 472–477.
- [56] M. Sprik, G. Ciccotti, *J. Chem. Phys.* **1998**, *109*, 7737.
- [57] J. Hutter et al., CPMD Program Package.

- IBM Corp 1990 – 2004, MPI für Festkörperforschung Stuttgart 1997 – 2001. See also <http://www.cpmc.org>.
- [58] J. P. Perdew, K. Burke, M. Ernzerhof, *Phys. Rev. Lett.* **1996**, *77*, 3865–3868.
- [59] D. Vanderbilt, *Phys. Rev. B* **1990**, *41*, 7892–7895.
- [60] S. Grimme, *J. Comput. Chem.* **2006**, *27*, 1787–1799.
- [61] M. Capdevila-Cortada, J. Ribas-Arino, J. J. Novoa, *J. Chem. Theory Comput.* **2014**, *10*, 650–658.
- [62] S. Nosé, *Mol. Phys.* **1984**, *52*, 255–268.
- [63] W. Hoover, *Phys. Rev. A* **1985**, *31*, 1695–1697.
- [64] G. J. Martyna, M. L. Klein, M. Tuckerman, *J. Chem. Phys.* **1992**, *97*, 2635.
- [65] C. Burisch, P. R. L. Markwick, N. L. Doltsinis, J. Schlitter, *J. Chem. Theory Comput.* **2008**, *4*, 164–172.
- [66] Gaussian09, RevisionD.01, M. J. Frisch, G. W. Trucks, H. B. Schlegel, G. E. Scuseria, M. A. Robb, J. R. Cheeseman, G. Scalmani, V. Barone, et al., **2009**.
- [67] R. Ditchfield, W. J. Hehre, J. A. Pople, *J. Chem. Phys.* **1971**, *54*, 724.
- [68] S. Miertuš, E. Scrocco, J. Tomasi, *Chem. Phys.* **1981**, *55*, 117–129.
- [69] E. Cancès, B. Mennucci, J. Tomasi, *J. Chem. Phys.* **1997**, *107*, 3032–3041.
- [70] E. D’Oria, J. J. Novoa, *CrystEngComm* **2008**, *10*, 423.
- [71] P. Kollman, *J. Am. Chem. Soc.* **1977**, *99*, 4875–4894.